Magnetic phases and reorientation transitions in antiferromagnetically coupled multilayers

U. K. Rößler* and A. N. Bogdanov†
Leibniz-Institut für Festkörper- und Werkstoffforschung Dresden, Postfach 270116, D-01171 Dresden, Germany
(Received 26 September 2003; published 28 May 2004)

In antiferromagnetically coupled superlattices grown on (001) faces of cubic substrates, e.g., based on material combinations as Co/Cu, Fe/Si, Co/Cr, or Fe/Cr, the magnetic states evolve under competing influence of bilinear and biquadratic exchange interactions, surface-enhanced fourfold in-plane anisotropy, and specific finite-size effects. Using phenomenological (micromagnetic) theory, a comprehensive survey of the magnetic states and reorientation transitions has been carried out for multilayer systems with even number of ferromagnetic sublayers and magnetizations in the plane. In two-layer systems ($N=2$) the phase diagrams in dependence on components of the applied field in the plane include ''swallow-tail-type'' regions of (metastable) multistate coexistence and a number of continuous and discontinuous reorientation transitions induced by radial and transversal components of the applied field. In multilayers ($N\geqslant 4$) noncollinear states are spatially inhomogeneous with magnetization varying across the multilayer stack. For weak fourfold anisotropy the magnetic states under influence of an applied field evolve by a complex continuous reorientation into the saturated state. At higher anisotropy they transform into various inhomogeneous and asymmetric structures. The discontinuous transitions between the magnetic states in these two layers and multilayers are characterized by broad ranges of multiphase coexistence of the (metastable) states and give rise to specific transitional domain structures.

DOI: 10.1103/PhysRevB.69.184420 PACS number(s): 75.70.−i, 75.50.Ee, 75.10.−b, 75.30.Kz

I. INTRODUCTION

Multilayers built from ferromagnetic layers with various spacer layers include a wide variety of magnetic film systems that have been intensively studied during past years. Due to remarkable phenomena as giant magnetoresistance, exchange-spring behavior and/or exchange bias, and surface enhanced magnetic anisotropy, such nanostructures have already found a number of applications and are considered as promising candidates for nonvolatile magnetic recording media.[1] On the other hand, nanoscale superlattices and similar structures provide convenient model systems to study different aspects of surface magnetism and magnetic ordering in confining geometry.

In particular, much attention has been given to multilayers composed of antiferromagnetically coupled ferromagnetic nanolayers.[2–18] Such layered synthetic antiferromagnets can be separated into two classes according to the symmetries ruling their magnetic properties. Superlattices with relatively strong uniaxial anisotropies include low-symmetry multilayers with effective uniaxial magnetic anisotropy in the layer planes, e.g., epitaxial systems deposited on (110) and (211) faces of cubic substrates.[3,4] Also multilayer systems with perpendicular anisotropy belong to this class.[5–7] Magnetization processes in these nanostructures are strongly influenced by the uniaxial anisotropy which is responsible for specific phenomena such as ''surface spin-flop''[3,8] or field-induced metamagnetic jumps.[5] On the other hand, the uniaxial anisotropy may be absent in layered systems with higher symmetry. These represent another large and intensively investigated class of synthetic antiferromagnetic nanostructures. Superlattices with planar magnetization grown on (001) faces of cubic substrates, e.g., multilayers from materials combinations as Co/Cu,[9] Fe/Si[10,11] Co/Cr,[12–14] or Fe/Cr[16–18] belong to this class. In the case of weak fourfold anisotropy, their magnetic properties are mostly determined by the interlayer exchange interactions which may include an important *biquadratic* contribution.[10,11,15–17] Evidence of strong biquadratic exchange interaction has been given in a number of experimental papers for Fe/Cr two-layers and multilayers,[15–17] for Fe/Si(001) multilayers.[11] Strong effective fourfold anisotropies have been found in systems such as Co/Cr(001) or Fe/Cr(001).[9,13,16,14] The competition between magnetic anisotropy, applied fields, and exchange energies may cause complicated magnetic effects and processes. In fact, a great number of novel magnetic configurations and remarkable reorientational effects in external fields have been found in such superlattices.[9,10,16,18] In particular, recent experimental results using modern depth-resolving techniques reveal spatially inhomogeneous magnetic structures, e.g., in Fe/Cr(001) superlattices,[18] and specific reorientation effects imposed by four-fold planar (tetragonal) anisotropy.[16] The understanding and interpretation of the complex magnetization processes found in such systems[19–21] requires a theoretical underpinning.

Theoretical activity in this field is largely based on analytical and numerical calculations mostly within phenomenological approaches.[3,8,16,22–24] These studies have demonstrated the general validity of the phenomenological models to describe the magnetization processes in antiferromagnetic nanostructures.[3,9,18,8] For the system under discussion the phenomenological theory has been developed to describe effects of biquadratic couplings[15] and a concomitant complex evolution of domain structures in Fe/Cr/Fe layers.[25] Fourfold anisotropy effects have been theoretically investigated in Ref. 23 for sandwich structures with $N=2$ ferromagnetic layers coupled through a spacer. Multilayer systems provide also experimental models to study effects of the confining surfaces on antiferromagnetic structures.[3,26] In this context, specific inhomogeneous magnetic states described for theo-

retical models in Ref. 24 have recently been observed in Fe/Cr superlattices.[18] The existing theoretical results, however, are restricted to special cases and are not sufficient for an exhaustive description of the magnetic states and field-induced reorientional effects observed in recent experiment.[9–14,16–18]

In this paper we provide a theoretical analysis of magnetic states and magnetization processes in planar antiferromagnetic superlattices with and without fourfold anisotropy in magnetic fields applied within the multilayer plane. In such magnetic superlattices the exchange interlayer coupling is an oscillatory function of the spacer thickness.[27,28] Depending on the spacer thickness an alternating sequence of ferromagnetic and antiferromagnetic interlayer couplings is realized, and, by adjusting the spacer thicknesses, very different strengths of antiferromagnetic coupling can be realized. On the other hand, the fourfold anisotropy includes interface-induced contributions, which implies a strong dependency of the effective average anisotropy of each ferromagnetic layer on the layer thickness.[29] Thus, the effective magnetic interactions can vary in extremely broad ranges for such multilayers in dependence on the chosen material combinations and thicknesses, see e.g. Ref. 9, where for a Co/Cu(001) two-layer system with a wedged spacer layer the ratio between fourfold anisotropy energy and the exchange coupling is changed by orders of magnitude. In contrast to bulk planar antiferromagnets, where an essentially fixed hierarchy for the strengths of the magnetic interactions holds,[30] in these artificial antiferromagnetic systems the ratios between different magnetic energies, respectively, the phenomenological parameters in the magnetic free-energy, may assume practically arbitrary values. Moreover, as the interlayer exchange is weak compared to direct exchange interactions, the fields to induce spin-reorientation phenomena are similarly weak and experimentally accessible.

The rich phase diagrams for these systems preclude an analysis in all details. The phase space in terms of the phenomenological parameters includes a large variety of different magnetic states with a corresponding multitude of spontaneous and field-induced phase-transformations. In a first step to such an analysis, all laterally homogeneous states in such multilayers must be found. They are the building blocks for a domain theory.[30,31] For the case of laterally homogeneous states of each ferromagnetic sublayer one has a system that behaves like an antiferromagnetically coupled chain of Stoner-Wohlfarth particles. This simplified one-dimensional model for the behavior across the multilayer stack also yields the limiting case for the magnetization processes with maximum hystereses. Again, a direct analysis of all magnetic states even for these one-dimensional models yields an intricate succession of phase diagrams and magnetization curves.[23] In this paper, we avoid the cumbersome task of listing and classifying *all* solutions and transitions. Instead, we provide a broad physically intuitive picture of the effects due to the different exchange or anisotropic forces, and those imposed by the confining geometry of the system. To this end, we study limiting cases of the model. This includes the case of strictly zero anisotropy with and without biquadratic exchange, and the case of infinite anisotropy with fixed fourfold orientation of the magnetizations in each layer. For the antiferromagnetic two-layer systems ($N=2$), i.e., the sandwich structures (experimentally realized as ferromagnetic/spacer/ferromagnetic trilayers), we provide a detailed investigation of the magnetic phase diagram for arbitrary orientation of fields in the layer planes. Based on this, we can understand the *basic* magnetic configurations in the multilayers, and we can give a map of the *topologically different types* of magnetic phase diagrams.

We use standard methods to analyze magnetic phases and transitions within the phenomenological approach and the theory of phase transitions.[32] The one-dimensional chain models are considered as composite order parameters with many components (N components in a multilayer stack composed of N ferromagnetic/spacer bilayers) and a characteristic structure of couplings between the components defined by interlayer exchange and the surfaces. From this point of view, the very rich phase diagrams and correspondingly complex sequences of magnetic configurations can be understood. For the general cases of the model, the equations for equilibrium and phase stability can be solved only by numerical methods. With the methods and results expounded below, one can extend the analysis to specific experimental cases in all detail.

The solutions for the one-dimensional chain models include various field-induced canted and inhomogeneous states with a net magnetization. Based on the phase diagrams of these models, the evolution of laterally inhomogeneous (domain) states and magnetization processes can be discussed.[31,30] In this connection, the coexistence regions of different phases in the vicinity of discontinuous (first-order) magnetic phase transitions are important. In external fields, thermodynamically stable domain configuration from these competing phases can be established in extended multilayers. This is crucial for an understanding of the hysteretic magnetization processes under coercivity mechanisms.

The paper is organized as follows. After introducing the model and mathematical tools (Sec. II) we consider the effects of the bilinear and biquadratic exchange interactions in the following section (Sec. III). In Sec. IV we investigate in detail fourfold anisotropy effects in antiferromagnetically coupled two-layers and then discuss the generalization of these finding to the case of multilayers. In Sec. IV we discuss domain states and magnetization processes by using qualitative arguments. In the concluding part we discuss possible extensions of the theory, and we suggest some useful experiments to enhance our understanding of magnetization processes in antiferromagnetic superlattices.

II. THE MICROMAGNETIC ENERGY

Let us consider a stack of N ferromagnetic plates infinite in x and y directions and with finite thickness along z axis. The magnetization of the layers is $\mathbf{M}_i$, and there are indirect interlayer-exchange couplings through spacers between them. The phenomenological energy of the system can be written in the following form:

$$\Phi_N = \sum_{i=1}^{N-1} [J_i \mathbf{m}_i \cdot \mathbf{m}_{i+1} + \tilde{J}_i (\mathbf{m}_i \cdot \mathbf{m}_{i+1})^2] - \mathbf{H} \cdot \sum_{i=1}^{N} \zeta_i \mathbf{m}_i - \frac{1}{2} \sum_{i=1}^{N} K_i (\mathbf{m}_x^4 + \mathbf{m}_y^4), \quad (1)$$

where $\mathbf{m}_i = \mathbf{M}_i / M_0^{(i)}$ ($M_0^{(i)} = |\mathbf{M}_i|$) are unity vectors along the ith layer magnetization. $\zeta_i = M_0^{(i)} / M_0$ designate deviations of the magnetization in the ith layer from the averaged value M_0. We assume that $\mathbf{m}_{iz} = 0$, i.e., the layer magnetizations are restricted to the layer plane. J_i and $\tilde{J}_i$ are constants of bilinear and biquadratic exchange interactions, respectively; K_i are constants of the in-plane fourfold anisotropy. The functional (1) generalizes similar models considered earlier in a number of studies on exchange[9,16,23,30] and anisotropy[16,17,22,25] effects in planar antiferromagnetic systems. Within this approach the ferromagnetic layers are considered as homogeneously magnetized blocks with constant values of the magnetic interactions. This assumption deserves some comment. It is well established that in magnetic nanostructures surface/interface exchange and relativistic interactions strongly modify electronic and magnetic properties within all volume of the magnetic constituents.[33] This means that the values of the exchange or anisotropy parameters, and the magnetizations include large interface/surface-induced components which may strongly vary across the thickness of the individual layers.[33,34] However, the hypothesis of magnetic homogeneity in the ferromagnetic nanolayers in the models of type (1) has a solid physical basis and is justified by successful applications of these models to describe magnetization processes in layered ferromagnetic and antiferromagnetic nanostructures.[3,8,9,16,18,34,35,36] This relies on the fact that in ferromagnetic nanolayers the intrinsic (direct) exchange coupling are usually very strong and overcome surface-interface-induced interactions. Thus, they play the dominating role to determine the magnetic order *within* the layers, which reacts also very stiffly on all external and induced magnetic forces. Furthermore, in these planar systems the stray field forces confine the magnetization of the layers into their plane. As a result, in most of these systems the ferromagnetic layers preserve essentially homogeneous in-plane magnetized states even under the influence of strongly inhomogeneous induced interactions.[34,35] In this connection it is important to stress here that the materials parameters in the phenomenological model (1) should be treated as averages over a multilayer *period*. They comprise (in integral form) all intrinsic and induced energy contributions of the magnetic states in the ferromagnetic layers. In particular, for the systems under consideration they may also include a contribution from magnetism of the spacer layers. Thus, in contrast to their bulk counterparts which are considered as constants of the magnetic materials, in nanoscale multilayer systems the phenomenological parameters strongly depend on many physical and geometrical factors and may considerably vary from sample to sample.

Parity of N also plays an important role. The model (1) with *even* number of ferromagnetic layers represents systems with fully compensated magnetization. Such superlattices can be treated as analogs to bulk collinear antiferromagnets. Superlattices with odd numbers of layers or with unequal thicknesses of layers own a noncompensated magnetization which strongly determines their global magnetic properties. In their response to an applied field, these structures are similar to bulk ferrimagnets. They could be studied by similar methods as used below, but have to be considered as separate class of systems. Concentrating on the properties of systems with fully compensated total magnetization, we consider only superlattices with even N and equal magnetization in all layers ($\zeta_i = 1$). In this contribution dedicated to general properties of these antiferromagnetic superlattices, we avoid secondary effects which are related to their microstructure and interface properties, such as strains, chemical intermixing, etc. With that in view we will study the model (1) mainly for the case of *identical* ferromagnetic layers assuming that the exchange and anisotropy constants are equal for all the layers, $J_i = J$, $\tilde{J}_i = \tilde{J}$, and $K_i = K$. Some of the analytical results can be generalized to the isotropic (i.e., with $K_i = 0$) system with mirror symmetry about the center of the layer stack, i.e., $J_i = J_{N-i}$ and $\tilde{J}_i = \tilde{J}_{N-i}$.

In our problem the magnetization of the ith layer is confined in planar orientations and can be described by the angle θ_i between the vector $\mathbf{m}_i$ and x axis. Thus, calculations of the magnetic states for the model (1) can be reduced to the optimization of the function $\Phi_N(\theta_1, \theta_2, \ldots, \theta_N)$. Following the theory of bulk antiferromagnetism it is convenient to introduce here the vectors of the *total magnetization* **m** and the *staggered* (or *antiferromagnetism*) vector **l**

$$\mathbf{m} = \sum_{i=1}^{N} \mathbf{m}_i, \quad \mathbf{l} = \sum_{i=1}^{N} (-1)^{(i+1)} \mathbf{m}_i. \quad (2)$$

The energy (1) is invariant under transformation $\mathbf{l} \rightarrow -\mathbf{l}$, and, therefore, all magnetic states in this model are degenerate with respect to the sign of the staggered vectors. In the following only solutions with a definite sign of the staggered vector will be discussed. However, one should keep in mind that the full set of solutions includes also those with opposite sign of **l**. The magnetic states with opposite sign of **l** behave identically in an applied magnetic field. Thus, for the magnetization processes there is no need to distinguish these solutions.

For the particular case of a two-layer ($N = 2$) the energy (1) can be transformed to the following form

$$\Phi_2 = J_1 \cos 2\phi + \tilde{J}_1 \cos^2 2\phi - 2H \cos\phi \cos(\theta - \psi) - \frac{K}{4} \cos 4\phi \cos 4\theta - \frac{3K}{4}, \quad (3)$$

where $\theta = (\theta_1 + \theta_2)/2$, $\phi = (\theta_1 - \theta_2)/2$ and ψ is the angle between the **H** and the x axis.

This case of a two-layer is of special interest. The energy (3) functionally coincides with that of a bulk two-sublattice antiferromagnet. This offers the opportunity for useful physical relations and analogies with bulk antiferromagnetism. On the other hand, the two-layers represent the simplest model of antiferromagnetically coupled layered nanostructures.

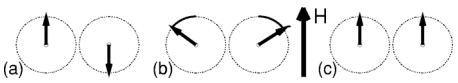

FIG. 1. Basic spin configurations in isotropic antiferromagnetically coupled two-layers ($N=2$). At zero field (a) the magnetization vectors $\mathbf{m}_i$ are antiparallel in adjacent layers but the structure has no fixed orientation in the plane (infinite degeneracy). An in-plane magnetic field lifts the degeneracy and stabilizes states with $\mathbf{l}$ perpendicular to the field and with $\mathbf{m}$ along the field—this is a spin-flop (SF) phase (b). In a sufficiently strong magnetic field the SF phases transform into the saturated (*flip*) phase (c).

The equations minimizing the function $\Phi_N(\theta_1,\theta_2,\ldots,\theta_N)$ have strongly nonlinear character and no analytical solution are available generally. The body of our results have been obtained by numerical methods. We solve the coupled equations for equilibria $\{\partial W/\partial\theta_i=0\}_{i=1,\ldots,N}$ by an efficient conjugate gradient minimization.[37] For systems with large anisotropy the configurations with the magnetizations oriented in the fourfold easy-axis directions are close to mostly metastable minima of the energy. These configurations have been systematically searched for global absolute stability and checked for stability. Numerically, this is feasible for N not too large with present day computers. Stability limits and phase transitions are determined from the evolution of the smallest eigenvalue $e_0(H,K)$ of the stability matrix $(\partial^2 W/\partial\theta_i\partial\theta_j),i,j=1,\ldots,N$ under changing parameters in Eq. (1), i.e., ratios $\tilde{J}/J$, K/J, or the applied magnetic field.

III. MAGNETIC STRUCTURES IN ISOTROPIC MULTILAYERS: SPATIALLY INHOMOGENEOUS SPIN-FLOP STATES

A. Exchange interactions in layered antiferromagnets

We start the investigations of the static configurations minimizing energy (1) from the isotropic case (i.e., with $K_i=0$). Depending on relations between bilinear and biquadratic constants different collinear and noncollinear configurations are stable.[22,25] The equations $J_i>0$, $\tilde{J}_i>0$, $J_i-2\tilde{J}_i>0$ determine the region in the parameter space where a collinear *antiferromagnetic* (AF) phase is the zero-field ground state consisting of blocks of adjacent layers with antiparallel orientation of the magnetization [Fig. 1(a)]. We restrict our analysis to this practically important case. The AF phase is infinitely degenerate with respect to orientations of the staggered vector $\mathbf{l}$ in planar directions.

The magnetic states for the isotropic two-layer ($N=2$) in the applied field can be obtained by minimization of the energy (3) with $K=0$. The solutions [$\theta=\psi$, $H=2(J-2\tilde{J})\cos\phi+8\tilde{J}\cos^3\phi$] describe the states with the staggered vector perpendicular to the applied field [so called *spin-flop* (SF) phase]. In an increasing magnetic field the magnetization vectors rotate into the field direction [Fig. 1(b)], and finally reaches a continuous transition into the ferromagnetic (*flip*) phase with $\tilde{\theta}=0$. This (*spin-flip* transition) occurs at

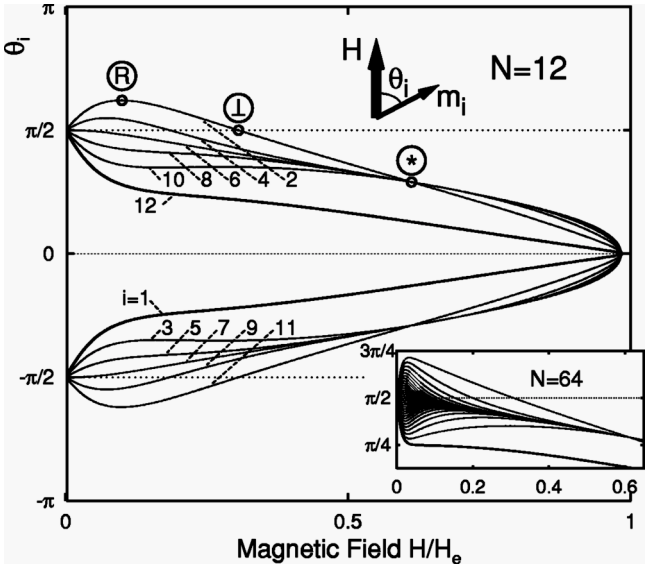

FIG. 2. Evolution of spin states in multilayers with a field H applied in the plane of the layers and for zero anisotropy $K\equiv 0$ and biquadratic exchange $\tilde{J}=0$, hence $H_e=4J$. Main figure: rotation angles of the layers in the plane θ_i ($i=1,\ldots,N$) for superlattice with $N=12$. At point labeled "R" the sense of rotation changes for the magnetization direction θ_i (here, $i=2$); at point "$\perp$" the magnetization of this layer is perpendicular to the applied field again. Point "*" is the "knot point" [Eq. (5)]. Inset: $N=64$ only θ_i for even $i=2$ and $i=4,8,12,\ldots,64$ shown.

the exchange field $H_e^{(2)}=2(J+2\tilde{J})$ [Fig. 1(c)], which is lower than the corresponding spin-flip field $H_e=4(J+2\tilde{J})$ for a bulk system.

In superlattices with $N\geqslant 4$ the magnetic field applied in the plane also lifts the degeneracy and stabilizes the SF phase (the state with $\mathbf{l}\perp\mathbf{H}$ and $\mathbf{m}\,||\mathbf{H}$) (Figs. 2–4). However, the magnetic configurations in these SF states and their evolution in the applied field are markedly different from those in bulk antiferromagnets or in the two-layer systems. It turns out that magnetic structures of the multilayers with N divisible by four ($N=4l$ called here *even-even*) differ from *even-odd* systems with $N=4l+2$ ($l=1,2,\ldots$). In low fields ($J_i-2\tilde{J}_i\gg H$) the solutions for the SF phase are given by a set of linear equations,

$$(J_{2j-1}-2\tilde{J}_{2j-1})(\pi-\theta_{2j-1}+\theta_{2j})=H,$$

$$\theta_{2j}-\theta_{2j+1}=0,\quad j=1,2,\ldots,l, \tag{4}$$

where $l=N/4$ for even-even and $l=(N+2)/4$ even-odd systems. It is clear that for the isotropic model the direction of the magnetic field in the film plane plays no role. Following the definition of the angles θ_i we assume here that the magnetic field is applied along the x axis. The solutions (4) describe small deviations of the magnetization vectors, from the directions perpendicular to the easy axis [see the magnetization profiles in Figs. 2 and 4 and the configuration in Fig. 3(b)]. In all internal layers ($i=2,\ldots,N-1$) neighboring pairs retain antiparallel orientations [e.g., $(\mathbf{m}_2,\mathbf{m}_3)$ and $(\mathbf{m}_4,\mathbf{m}_5)$ in Fig. 3(b)]. For even-even systems the magneti-

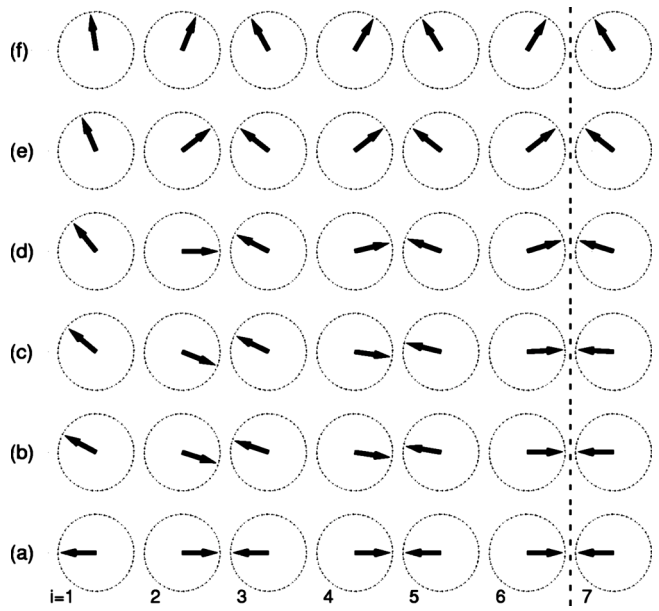

FIG. 3. Spin states in multilayers with $N=12$ for zero anisotropy $K\equiv 0$ and field H applied in the plane: (a) $H=0$, (b) $H<H_R^{(2)}\ll H_e$, (c) $H=H_R^{(2)}$, (d) $H=H_\perp^{(2)}$, (e) $H=H^*$, and (f) $H^*<H<H_e^{(N)}$, i.e., below the transition to the flip phase (cf. Fig. 2). All states have mirror symmetry about the center of the multilayer stack (marked by the dashed line).

zation vectors of the central layers ($\mathbf{m}_{N/2}$, $\mathbf{m}_{N/2+1}$) preserve perpendicular orientation even in finite (but weak) fields (see layers 6 and 7 in Fig. 3). For even-odd systems the magnetization vectors of all layers have finite deviations from perpendicular orientation. Towards top and bottom layer $i=1$ or

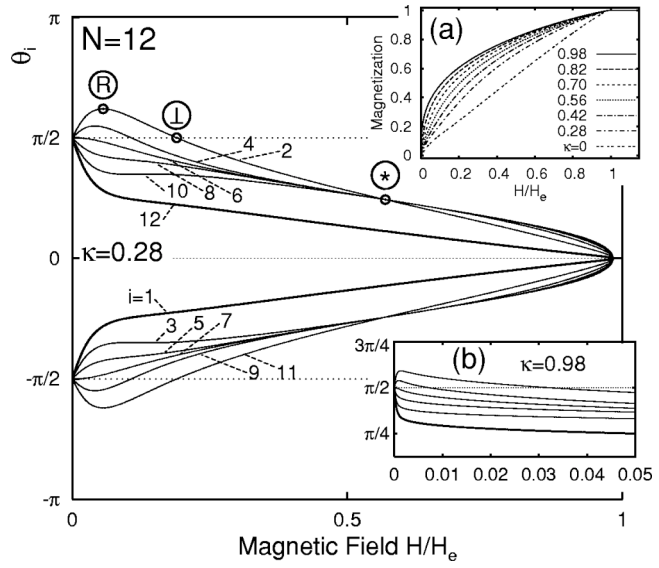

FIG. 4. Evolution of magnetic states in antiferromagnetic multilayer $N=12$ with zero anisotropy $K\equiv 0$ and biquadratic exchange $\kappa=2\tilde{J}/J>0$, i.e., with enhanced $H_e=4(J+2\tilde{J})$ (compare with Fig. 2 for $\kappa=0$). H is applied in the layer plane. (a) Magnetization curves in the range of values of κ with antiferromagnetic ground state in zero field. (b) Evolution of states (only shown for layers with even numbers) in small fields for $\kappa=0.98$.

N in the stack, these deviations increase. Due to antiparallel orientation the pairs have zero net magnetization. The total magnetization arises only due to the top and bottom layers $i=1$ and N. Note that in these configurations a number of layers rotates against the applied field (in Figs. 2–4 the layers with $i=2$, 4 and their symmetric counterparts with $i=11$, 9). This occurs because, in weak fields, the exchange interactions favoring antiparallel magnetizations in adjacent layers play the dominant role. An increasing magnetic field counteracts and slows down this reverse rotation, when the nonlinear evolution for the magnetization structure is reached, and finally the sense of rotation is changed at characteristic fields $H_r^{(i)}$ where $d\theta_i/dH=0$. With increasing N the number of layers increases which display this reverse rotation, the deviations from orientations perpendicular to the applied low field become larger near the surface layers, and the fields $H_r^{(i)}$ are reached at lower fields (see inset in Fig. 2 for $N=64$). A further set of characteristic fields $H_\perp^{(i)}$ defines the points where the projection of $\mathbf{m}_i$ on the field directions changes the sign (the field $H_r^{(2)}$ and $H_\perp^{(2)}$ are indicated in Fig. 2). In increasing field these characteristic fields initially are reached for the central layers and at higher fields for those closer to the boundaries. For fields $H>H_\perp^{(2)}=H_\perp^{(N-1)}$ the magnetization directions of all layers have positive projections onto the field direction. In the model with equal exchange constant there is another special field H^* (independent of N), where all inner layers have the same projection onto the field direction $[\theta_i=(-1)^{i+1}\theta_0^*,\ i=2,3,\ldots,N-1]$. The parameters of this ''knot'' point are determined from a set of equations,

$$H^*=4(J+2\tilde{J})\left(1-\frac{2\kappa}{1+\kappa}\sin^2\theta^*\right)\cos\theta^*,\quad \sin\theta^*=2\sin\theta_1^*,$$

$$\cos\left(\frac{\theta_1^*+3\theta^*}{2}\right)+\kappa\cos\left(\frac{\theta_1^*-\theta^*}{2}\right)\cos(\theta_1^*+3\theta^*)=0,$$

$$\kappa=2\tilde{J}/J. \tag{5}$$

The functions $H^*(\kappa)$, $\theta_1^*(\kappa)$, and $\theta^*(\kappa)$ are plotted in Fig. 5. In particular, for superlattices with zero biquadratic exchange $\tilde{J}=0$ one has $H^*=\sqrt{6}\,H_e/4$ and $\theta^*=\arccos(\sqrt{3/8})$. Near saturation, the SF phase has only positive projections of the magnetization on the direction of the magnetic field which decreases towards the center similar to spin configurations obtained numerically in Ref. 24.

The spatial inhomogeneity of the SF phases in the multilayers and their remarkable evolution in the applied field are due to the particular *finite-size* effects in this type of magnetic nanostructures. In such layered nanostructures all internal layers interact with two adjacent layers but the top and bottom layers have only one neighboring layer. Thus, their exchange coupling is weakened compared to internal layers within the multilayer stack. This strong disbalance of the exchange forces at the boundaries affects the magnetic ordering within the entire multilayer and causes the reorientational processes in the SF phases. This mechanism is also responsible for the occurrence of inhomogeneous states in other

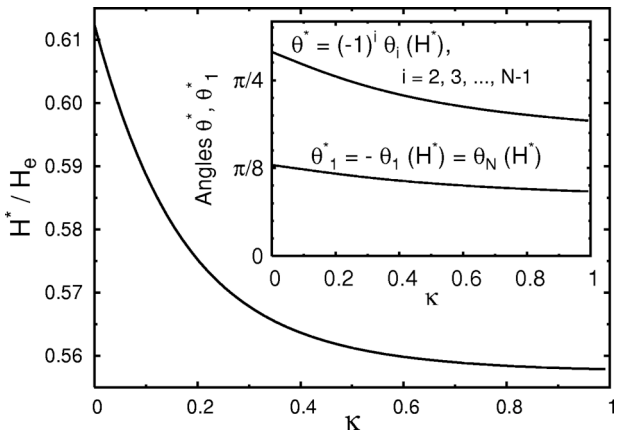

FIG. 5. Dependence of knot point H^* [Eq. (5)] on strength of biquadratic exchange κ. Inset shows the two angles θ^*, θ_1^* which characterize this special configuration independent on N.

noncollinear structures in the multilayers (see Secs. IV C and V A). Note that this important role of the cut exchange couplings is specific to antiferromagnetic confined systems with noncompensated moments at surfaces. In contrast, the cutting of exchange couplings does not affect *ferromagnetically* coupled nanostructures where relative orientation of the magnetization in the layers essentially depend only on magnetic anisotropy, applied fields, and the demagnetizing stray fields.

B. Effects of the biquadratic exchange

Evolution of spin-flop profiles for the multilayer with finite biquadratic exchange is plotted in Fig. 4. For the systems with collinear ground states the biquadratic exchange does not induce reorientional transitions but it has rather strong influence on the distribution of the magnetization in the multilayers (see insets in Fig. 4) and the value of the characteristic fields (Fig. 5). The effects of a biquadratic exchange $\tilde{J}>0$, if present in multilayers with collinear antiferromagnetic ground state, can be easily understood. For magnetic configurations close to the antiparallel orientation of neighboring layers, it softens the linear exchange forces; for nearly parallel orientation the system becomes stiffer instead. The evolution of the magnetic states in the external field is distorted accordingly by the presence of the biquadratic exchange $\tilde{J}>0$ (Fig. 4). In low fields close to the antiferromagnetic ground state, the system reacts more strongly on the external field. Thus, the fields $H_r^{(i)}$, where the rotation of the ith layer reverses, and the field $H_\perp^{(i)}$, where perpendicular orientation with respect to field is regained, respectively, are reached at relatively lower fields (labels "R" and "$\perp$" in Fig. 4). Conversely, the ferromagnetic state is reached only close to the enhanced exchange fields H_e, reflecting the stiffening of the effective exchange couplings in nearly ferromagnetic configurations. Thus, the magnetization curves acquire a nonlinear character with increasing $\tilde{J}>0$ [inset (a) in Fig. 4]. Experimental observation of the fields $H_r^{(i)}$ and the special field H^* (Fig. 5) could be used to determine the relative strength of $\tilde{J}>0$. For large values of $\tilde{J}$ the reversal

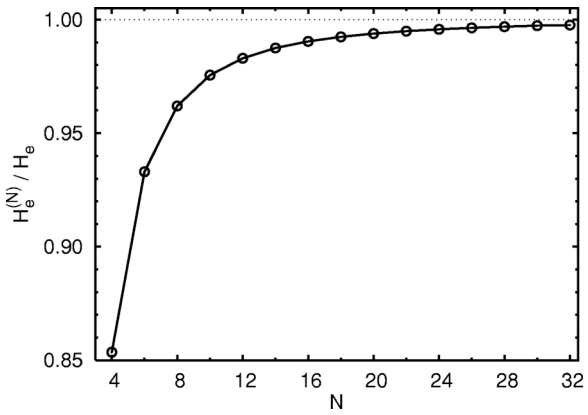

FIG. 6. Spin-flip fields for antiferromagnetic multilayers (zero anisotropy $K\equiv 0$) in dependence on number of layers N.

of the rotation of the magnetizations of individual layers takes place at very low fields [see inset (b) in Fig. 4].

C. Spin-flip transition

Near the spin-flip transition from the SF phase to the ferromagnetic states, the deviations of $\mathbf{m}_i$ from the field directions are small ($\theta_i \ll 1$), and the energy of the system (1) can be expressed by the quadratic form $W=\Sigma_{i,j=1}^{N} A_{ij}\theta_i\theta_j$, where the matrix A_{ij} has a tridiagonal band structure with nonzero elements only in the main diagonal $A_{ii}=H-\overline{J_i}$ and with the side diagonal elements $A_{i,i-1}=A_{i-1,i}=J_i+2\tilde{J}_i \equiv \overline{J_i}$. The spin-flip field $H_e^{(N)}$ is determined as the largest root of the equation $\det(A_{ij})=0$. In particular, for the model with equal parameters these solutions are plotted in Fig. 6. The spin-flip field gradually increases from $H_e^{(2)}=2(J+2\tilde{J})$ for the two-layer to the "bulk" value $H_e=4(J+2\tilde{J})$ in the limit of infinite N (Fig. 6). This dependence reflects the increase of the average number of exchange bonds from the value 1 for the two-layer and approaching 2 as N tends to infinity.

IV. EFFECTS OF TETRAGONAL ANISOTROPY IN TWO-LAYER SYSTEMS

Effects of the fourfold magnetic anisotropy on the states in the antiferromagnetic superlattices are revealed in detail by applying fields in arbitrary directions. We approach the general case by a detailed investigation on the case of the two-layer. To set the stage, we discuss the highly symmetric phase diagrams with fields in direction of easy and hard axes in the plane. This completes earlier work by Dieny *et al.*[23] on the $N=2$ systems. Then, we present phase diagrams for arbitrary field directions in the layer plane. As we have seen in the preceding section, the primary effect of biquadratic exchange is a distortion of phase diagrams in various regions. Thus, here we consider only models with $\tilde{J}=0$ to avoid such quantitative effects which will not affect the general topological features of the phase diagrams.

Optimization of the function $\Phi_2(\theta,\phi)$ [Eq. (3)] yields solutions for the magnetic states and their stability limits. In

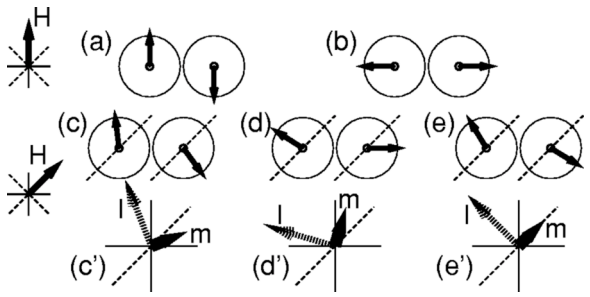

FIG. 7. Magnetic configurations in planar antiferromagnetically coupled two-layers with fourfold anisotropy. Easy directions are indicated by thin continuous lines, and hard directions by dashed lines. In zero field two antiferromagnetic configurations (I) (a) and (II) (b) with the staggered vectors along the easy directions correspond to the ground state. A magnetic field along the hard directions distorts them into the canted phases (c) and (d) which transform into the spin-flop state (e). Corresponding configurations of net magnetization and staggered vectors are shown for the two canted phases (c′) (d′), and for the spin-flop phase (e′).

zero field the tetragonal anisotropy lifts the rotational degeneracy of the AF phase and stabilizes two different states with perpendicular orientations of **l** [Fig. 7(a)].

A. Magnetic field along hard directions

In a field applied along one of the hard axes, the AF configurations of the ground state [Figs. 7(a) and 7(b)] are distorted into low-symmetry configurations [so-called *canted* phases—Figs. 7(c) and 7(d)]. Both these magnetic configurations preserve mirror symmetry with respect to the field direction and have the same energy. The total magnetizations **m** of these canted states deviate from the field directions to different sides at equal angles [Figs. 7(c′) and 7(d′)]. An oblique magnetic field deviating from the hard direction to one or the other side violates the phase balance between these two canted states. It favors the canted phase with the larger projection of **m** onto the field direction. This is the typical situation of a first-order (or discontinuous) transition.

In an increasing field the vectors **m** in both canted phases rotate into the field direction and reach it at a certain critical field H_{sf1}. At this point both phases transform into the common configuration corresponding to the SF phase [Fig. 7(d)], i.e., a second-order (or continuous) phase transition from low-symmetry canted phases into the high-symmetry SF phase occurs in this field. Standard analysis yields the following expression for the parameters of the critical point

$$H_{sf1}=(J+K\nu)\sqrt{2(1+\nu)},$$

$$\nu=(1+k-\sqrt{1+14k+25k^2})/(6k),\quad k=|K|/J, \qquad (6)$$

where $\nu=\cos\phi_{sf}$ determines the equilibrium SF configuration at the critical field.

The two canted phases are competing phases related by a first-order transition. At the field H_{sf1} the discontinuity between these phases disappears, i.e., this is a *critical point* terminating the first-order transition. After the transition into the SF phase, the system further evolves by rotation of the magnetizations $\mathbf{m}_i$ into the direction of the field. This process is terminated at another critical field $H_{f1}=2J(1+k)$ (Fig. 8).

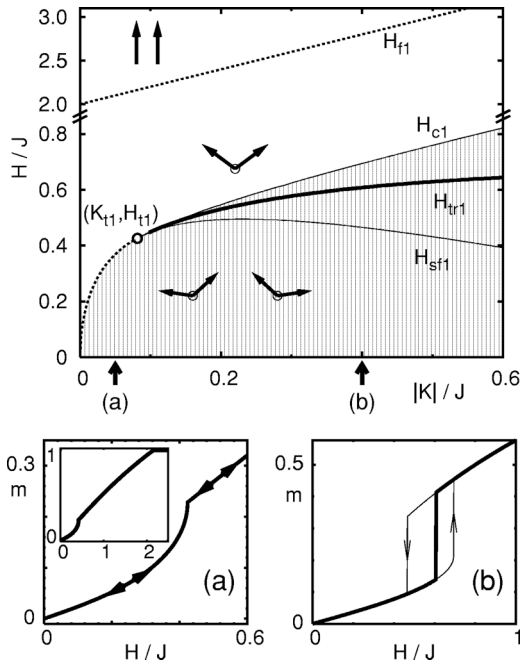

FIG. 8. Magnetic phase diagram of the two-layer system in magnetic fields along *hard* directions. The tricritical point ($K_{t1}=0.081\,406\,J$, $H_{t1}=0.425\,780\,J$) separates the continuous (dotted line) and discontinuous (thick line) transitions between the canted and SF phases. A further dotted line gives the critical field of the second-order transition between the SF and flip phases H_{f1} (6). Thin lines give the lower stability limit H_{sf1} of the SF phases and the upper limit H_{c1} of the canted phases. The gray area is the region of the phase equilibrium between the two canted phases [see Figs. 7(c) and 7(c′) and 7(d) and 7(d′)]. Magnetization curves for low and high anisotropy, as indicated in the main panel, are plotted in (a) and (b).

The transition between the canted and SF phases is continuous only below a certain anisotropy strength, $|K|<K_{t1}$, and becomes discontinuous at higher anisotropy. The parameters of the corresponding tricritical point $K_{t1}=0.081\,406\,J$, $H_{t1}=0.425\,780\,J$ have been calculated numerically from the equation $K_{t1}=(1+\nu)/(6\nu^2-2\nu-4)$ together with Eq. (6). Numerically calculated transition fields H_{tr1} and the upper stability fields of the canted phases H_{c1} are plotted in Fig. 8. In this picture the gray area describes the region of the first-order transition, respectively, the region of phase coexistence between the canted phases.

B. Magnetic field along easy directions

A magnetic field applied in one of the easy directions violates the energy balance between the two AF states. The state AF(I) with staggered vector parallel to the field does not change its configuration and exists as a metastable collinear state up to the critical field H_{af}. The phase AF(II) with the staggered vector perpendicular to the magnetic field transforms into a SF phase which corresponds to the global en-

ergy minimum of the system. In an increasing magnetic field this phase evolves similar to the SF phase along the hard directions, and continuously transforms into the flip states at the critical fields H_{f2} for low anisotropy.

The transition between the SF and flip phases changes the order in another tricritical point (K_{t2},H_{t2}). At a critical field H_{sf2} (7) the SF phase becomes unstable with respect to flipping distortions, i.e., modes that redirect the magnetization vectors into the field direction but preserve the symmetry of the SF phase. The parameters of the tricritical point $[|K|_{t2}=(1/5)J, H_{t2}=(8/5)J]$ and the stability limits

$$H_{af}=2J\sqrt{k(1+k)},\quad H_{sf2}=\frac{2J}{3}\sqrt{\frac{2(1+k)^3}{3k}},$$

$$H_{f2}=2J(1-k) \tag{7}$$

have been calculated in Ref. 23. After some algebra the first-order transition field H_{tr2} also can be derived in analytical form,

$$H_{tr2}=\frac{8J}{9}\left[1+\frac{(3+k)}{12}\left(\sqrt{1+\frac{3}{k}}-1\right)\right], \tag{8}$$

At the transitional field we have $\cos\phi=(\sqrt{1+3/k}-1)/3$. The (K,H) phase diagram for this cases is plotted in Fig. 9.

With increasing strength of the anisotropy, the ''landscape'' described by the energy function $\Phi_2(\theta,\phi)$ acquires additional folds. In particular, metastable canted phases arise in a certain region of the magnetic fields along the easy directions. (This region is indicated by gray color in Fig. 9). For $|K|/J\equiv k>k^*$ with $k^*=0.28+0.08\sqrt{6}=0.475\,96$ the SF phase undergoes an instability with respect to a transition into the canted phases. This instability occurs at lability fields which are given by the two branches of the following parametric equation:

$$H_{sf2}^{(1,2)}=(J-|K|\nu_{1,2})\sqrt{2(1+\nu_{1,2})},$$

$$\nu_{1,2}=(k-1\mp\sqrt{1-14k+25k^2})/(6k), \tag{9}$$

where $\nu_{1,2}$ is given by the the configuration in the SF state, $\nu_{1,2}=\cos 2\phi_{sf2}$. Both branches of the lability field (9) start at the point $H_{sf2}^{(1,2)}(k^*)=1.3895J$ (point □ in Fig. 9); $H_{sf2}^{(2)}$ meets the lability line H_{sf2} of Eq. (7) at the ''beak'' $(k=1/2, H=\sqrt{2}J)$ (point △ in Fig. 9). The transition between the metastable SF phase and the metastable canted phases along $H_{sf2}^{(1,2)}$ is continuous between the points △ and a further tricritical point ○. For stronger anisotropy the transition between these metastable phases is discontinuous at a first-order transition field H_{tr3}. This transition line along with the stability limits of the canted phases have been numerically determined as given in Fig. 9. Note that such processes between metastable phases may be realized only in systems with high coercivity where the transition into the thermodynamically stable flip phase is suppressed at the field H_{tr2} (8).

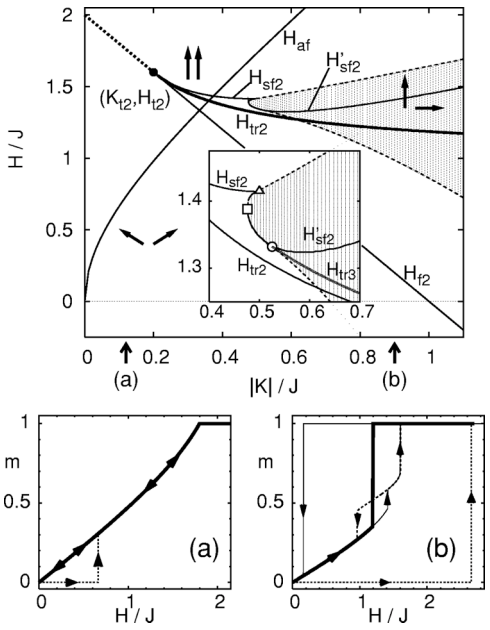

FIG. 9. Magnetic phase diagram of the two-layer system in magnetic fields along *easy* directions. The tricritical point $[K_{t2}=(1/5)J,\ H_{t2}=(8/5)J]$ separates the continuous H_{f2} (7) (dashed line) and discontinuous H_{f2} (8) (thick line) transitions between SF and flip phases. The tricritical point $(K_{t2}=0.2J,\ H_{t2}=1.6J)$ separates the continuous H_{f2} (7) (dashed line) and discontinuous H_{f2} (8)(thick line) transitions between SF and flip phases. Thin lines indicate the lability lines of the individual phases (7). The gray area designates the stability region of the canted phases. For the anisotropy $|K|/J=k^*=0.475\,96$ (point □), the critical field of the SF phase switches from an instability against symmetric ''flipping'' at the line H_{sf2} to an instability against canting at H'_{sf2} given by the two branches $H_{sf2}^{(1,2)}$ from Eq. (9). [Inset in the main figure shows the details of this process; see text following Eq. (9) for further explanation.] Small panels (a) and (b) show magnetization curves for low and high anisotropies as indicated in the main figure. Full thick lines are for the evolution of the equilibrium ground states, in (a) from SF phase to a continuous spin-flip transition into saturation. Dotted lines are the evolution starting from the metastable AF phase. In (b) the evolution of the saturated state in decreasing fields is given by a thin line. The inner small hysteresis loop shows the transitions from and into the metastable canted phase.

C. Evolution of (H_x,H_y) phase diagrams

Now we consider the magnetic states in applied fields deviating from the symmetric directions and construct (H_x,H_y) phase diagrams for different values of the parameter $k=|K|/J$. For the (H_x,H_y) diagrams in Figs. 10 to 14 it is assumed that the easy directions coincide with the x and y axis. This corresponds $K>0$ in the energy Eq. (3). Diagrams for $K<0$ can be obtained by rotation of those for $K>0$ through an angle $\pi/4$. In the limit of weak anisotropy, $|K|\ll J$, independent minimization with respect to the angle ϕ yields $2J\cos\phi=H\cos(\theta-\psi)$ and the energy (3) is simplified to the following form:

$$F(\theta)=-\frac{H^2}{2J}\cos^2(\theta-\psi)-\frac{K}{4}\cos 4\theta\left[1-\frac{2H^2}{J^2}\cos^2(\theta-\psi)\right]. \tag{10}$$

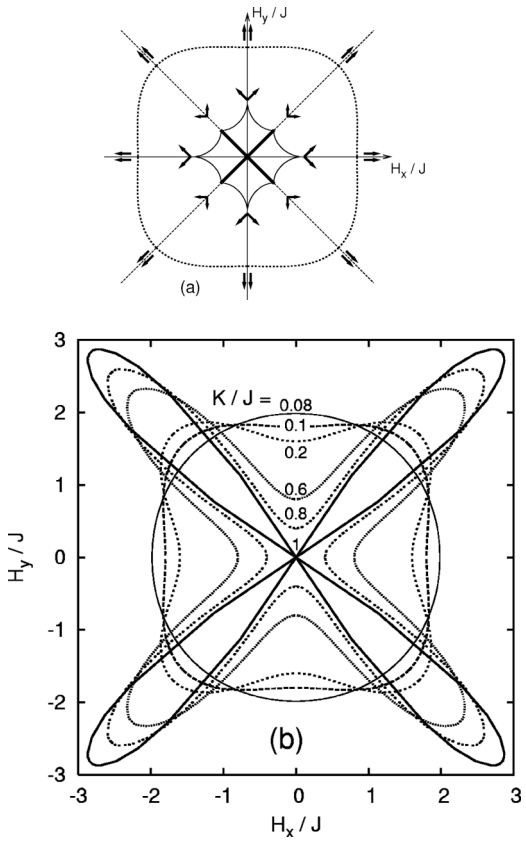

FIG. 10. (a) Schematic (H_x, H_y) phase diagram of the two-layer for $0<K<K_{t1}$. The astroid (continuous line) gives the stability limit of the canted metastable phases. Thick lines in diagonal directions (hard axis) are first-order transitions between canted phases. The line for the (continuous) transition into the saturated spin-flip state is given by the dotted line. Note that the real size of the astroid in the (H_x, H_y) diagram is much smaller than shown here. (b) Evolution of spin-flip field, respectively, lower stability limits of the saturated (ferromagnetic) phase (FM). Phase FM is stable outside the closed curves for the various values of anisotropy $0<K<1$. For $K/J>1.0$ the FM phases are (meta)stable even in reverse fields and the existence regions overlap for states saturated in different easy directions.

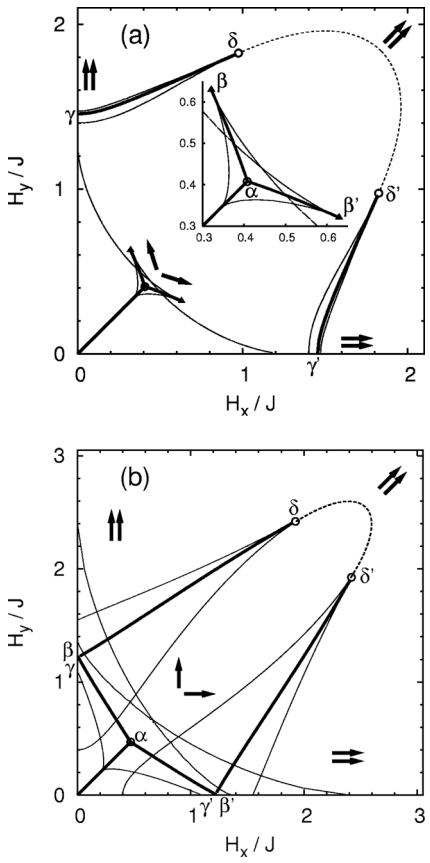

FIG. 11. First quadrant of the (H_x, H_y) phase diagram for antiferromagnetic two-layers with (a) $K=0.3J$ and (b) $K=0.8J$. Easy axes of magnetic anisotropy are along the axes of the diagrams. Inset in (a) magnifies the region of the swallow tail for the discontinuous transitions in magnetic fields oriented close to the hard axes. Thick lines are lines of first-order transitions. The dotted lines δ–δ' are continuous spin flips from spin-flop phase to the saturated (spin-flip) state. Thinner lines are the limits of stability, defining the coexistence regions for the corresponding phases.

The set of equations for the stability limits of solutions, $dF(\theta)/d\theta=0$ and $d^2F(\theta)/d\theta^2=0$, yield two closed lines of critical fields in the (H_x, H_y) phase diagram (Fig. 10). One of them $H=2(J-K\cos 4\psi)$ describes the second-order transition into the flip phase with $\phi=0$. The other closed curve can be written in a parametric form:

$$H^2\cos(2\theta-2\psi)=4KJ\cos 4\theta-K^2\Omega_1(\theta),$$

$$H^2\sin(2\theta-2\psi)=2KJ\sin 4\theta-K^2\Omega_2(\theta), \qquad (11)$$

where $\Omega_1(\theta)=4[7\cos^2 4\theta-2-2\mathrm{sgn}(K)\cos 4\theta\sqrt{3\cos^2 4\theta+1}]$, $\Omega_2(\theta)=2[5\sin 4\theta-2\mathrm{sgn}(K)\sin 4\theta\sqrt{3\cos^2 4\theta+1}]$. It describes an astroid with eight cusps that confines the region of the canted metastable states [Fig. 10(a)]. The cusps along the easy directions coincide with the stability field of the AF phase H_{af} Eq. (7), and those along the hard directions with $\tilde{H}_{sf1}$, [Eq. (6)]. Thick black lines within the astroid and along the hard directions indicate the first-order transitions between the canted phases from Fig. 7. This topology of the (H_x, H_y) phase diagram [Fig. 10(a)] is preserved up to the first tricritical point K_{t1}. For $|K|\geqslant K_{t1}$ a first-order transition between SF phase and two canted phases arises along the hard directions [point α in Fig. 11(a)]. For stronger anisotropies, $|K|>K_{t1}$, discontinuous phase transitions exist also for finite deviations of the field direction from the hard axes. The corresponding line of these first-order transitions have critical end points, where the difference between the competing phases disappears (analogous to the end point of a coexistence line in gas-liquid phase diagrams). For $|K|\geqslant K_{t2}$ and for fields along the easy directions, the spin flip into the saturated (induced) ferromagnetic state occurs discontinuously. Thus, another line of first-order transitions develops for $|K|>K_{t2}$ also in oblique fields. Correspondingly, the transition lines for spin flips in (H_x, H_y) phase diagrams consist of continuous and discontinuous sections joined by the tricritical points δ, δ'. The calculated (H_x, H_y) phase diagrams for

$K=0.3J$ in Fig. 11(a) and for $K=0.8J$ in Fig. 11(b) represent the main topological features of these phase diagrams. Point α indicates the field of phase equilibrium between the SF phase and two canted phases and corresponds to the critical field H_{tr1} from Fig. 8; points β and β' are the end points of the first-order transitions between one of the canted phases and the SF phase. Points $\gamma\gamma'$ correspond to the transition field H_{tr2} from Fig. 9; points δ and δ' are the tricritical points, where the discontinuous transition between the flip phase and the distorted SF phase ends. The lability lines in the vicinity of the transition field H_{tr1} have the shape of a ''swallow tail.'' Similar phase diagrams arise in uniaxial ferromagnets with strong fourth-order anisotropy.[38,39] As the anisotropy constant increases in the region $|K|>K_{t2}$ the lines of the first-order transitions extend, and near the special value $|K|/J=k^*=0.476$ the points β, β' reach the easy directions. For larger $|K|$ canted phases exist as metastable state also for fields in easy directions (compare Fig. 9). However, for increasing fields close to this direction, the discontinuous transition from the spin-flop state into the spin-flip state occurs before the transition into such a canted phase can take place, i.e., the two first-order lines $\alpha-\beta$ and $\delta-\gamma$ cross each other close to the easy-axis directions in Fig. 11(b). Bröhl *et al.*[9] reported evidence of an intermediate canted state in a Co/Cu/Co/Cu(001) system with field in an easy direction, following the theoretical prediction of such states by Dieny *et al.*[23] However, the state was found at lower fields than expected. This may be due to a misorientation of the external field and/or a mosaic of the epitaxial layer system because then the canted state becomes stable already at lower fields, as can be seen from line $\alpha-\beta$ in phase diagram Fig. 11(b). Generally, it is not sufficient to investigate only magnetization behavior in hard- and easy-axis directions for a thorough understanding of the magnetization phases in these multilayer systems.

To understand the transformation of (H_x,H_y) diagrams with increasing tetragonal anisotropy, the limiting case is useful where $\mathbf{m}_i$ are strictly oriented along the easy axes. In this case with *infinite* anisotropy, i.e., $|K|=\infty$, our model can be considered as a chain of an antiferromagnetic four-state clock model or planar Potts model[40] in a transverse external field. Recently, such four-state clock models were employed to analyze the spin configurations of bulk tetragonal metamagnets with large fourfold anisotropies, such as rare-earth nickel borocarbides[42,41] or rare-earth silver antimonides.[43] Rich experimental (H_x,H_y) phase diagrams have been obtained and analyzed in terms of four-state clock models, e.g., for $HoNi_2B_2C$[42] or $DyAgSb_2$.[43] The values of the angles $\theta_i=0$, $\pi/2$, π, or $3\pi/2$ in these fourfold states for $K=\infty$ are symbolically given by $\uparrow$, $\leftarrow$, $\downarrow$, and $\rightarrow$; e.g., the AF and SF phases are $(\uparrow\downarrow)$ and $(\rightarrow\leftarrow)$ for $N=2$. In addition to the collinear AF and flip states there are phases with perpendicular orientation of the magnetization, or ''90° folded'' phases (Fig. 12). The states created by all combinations of these four angles θ_i for the magnetization in the multilayer stack exist as metastable states in arbitrary magnetic fields because the energy wells corresponding to these solutions are separated by infinitely high potential barriers. The regions of the absolute stability of these phases are separated by first-order transitions lines shown in Fig. 12. In the first quadrant the transition between the AF states and the canted phase $(\uparrow\rightarrow)$ occurs at the line $H_x+H_y=J$; the transitions lines from the canted phase $(\uparrow\rightarrow)$ into the flip states $(\uparrow\uparrow)$ and $(\rightarrow\rightarrow)$ are $H_y-H_x=J$ and $H_y-H_x=-J$, correspondingly (Fig. 12). In the points (1,0) and (0,1) four phases coexist. Thus, under increasing strength of the anisotropy $(K>0)$ the (H_x,H_y) phase diagram evolves from that plotted in Fig. 10(a) for $K\ll J$ to that in Fig. 12 for infinitely large values of K.

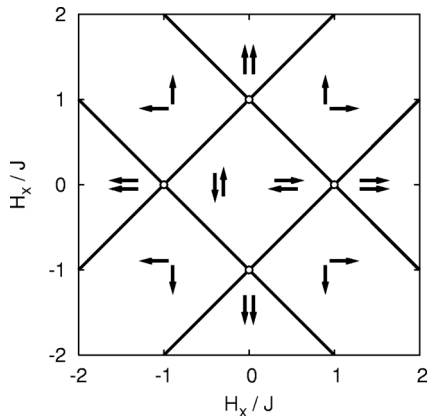

FIG. 12. (H_x,H_y) phase diagram of the $N=2$ layer system in the limit of an infinite positive fourfold anisotropy.

V. MAGNETIZATION CONFIGURATIONS AND PROCESSES IN MULTILAYERS

The equilibrium magnetic configurations in two-layer systems arise as a results of the competition between the interlayer exchange coupling and tetragonal anisotropy. For multilayers the disbalance of the exchange forces at the boundaries (Sec. II) additionally influences the magnetic states. We first describe the structure of the one-dimensional solutions for laterally homogeneous states in finite antiferromagnetic superlattices. These magnetic states are determined by the interplay between cut exchange at the surfaces and the fourfold anisotropy. Then we discuss some consequences for multidomain states and magnetization processes, and we discuss the physical nature of other effects which may play a role for the magnetic behavior of real experimental systems.

A. Exchange cut versus tetragonal anisotropy

First, we investigate the (H_x,H_y) diagrams of magnetic states of multilayers with $N\geqslant 4$ in the limit of infinite fourfold anisotropy. The zero-field ground states are the AF phases $(\uparrow\downarrow\ldots\uparrow\downarrow)$ and $(\rightarrow\leftarrow\cdots\rightarrow\leftarrow)$. We may restrict the field to be oriented in directions ψ in the interval $[0,\pi/4]$. The configurations for other values of ψ follow from symmetry. Then, we may distinguish the four ground-state (zero-field) domains $(\mathrm{AF1})^{(n)}=(\uparrow\downarrow)^{(n)}$, $(\mathrm{AF2})^{(n)}=(\downarrow\uparrow)^{(n)}$, $(\mathrm{SF1})^{(n)}=(\rightarrow\leftarrow)^{(n)}$, and $(\mathrm{SF2})^{(n)}=(\leftarrow\rightarrow)^{(n)}$, where n signifies the number of repetitions of the pair in a domain. In external fields $H>0$ configurations with net magnetization will be stabilized. These configurations must

have pairs of adjacent moments flipped by 90° $L=(\uparrow\rightarrow)$ or $X=(\leftarrow\uparrow)$, and by 180° $F=(\uparrow\uparrow)$. The 90° folded configuration X is less favorable than L for field orientations in the chosen range, except for fields in easy-axis direction $\psi=0$. Thus, the magnetized configurations with lowest magnetization and smallest expense of exchange energy are those with only one pair of type L. In a short-hand, we write $L^{(1)}$ for these configurations of type $(\mathrm{AF1})^{(n)}/L/(\mathrm{SF2})^{(N/2-n-1)}$ (with $n=0,1,\ldots$). Next, we may form configurations with higher magnetization and smallest expense of exchange energy using one L and one X pair: $L^{(1)}X^{(1)}=(\mathrm{AF1})^{(n)}/L/(\mathrm{SF2})^{(N/2-n-m-2)}/X/(\mathrm{AF1})^{(m)}$ $(n,m=0,1,\ldots)$. These configurations have the same energy and, therefore, are degenerate with configurations containing only one F pair: $F^{(1)}=(\mathrm{AF1})^{(n)}/F/(\mathrm{AF2})^{(N/2-n-1)}$. Note that these states are highly degenerate because the L, X, or F pair may be placed at arbitrary positions in the stack of N layers. In higher fields configurations with various combinations of L, X, and F pairs may be stabilized by an external field. However, the structures with lowest energy, i.e., the absolutely stable states, are rather simple because of the following considerations. If, in external fields, more than one L pair can be formed starting from the $L^{(1)}$ structure, the formation of the maximum number of L pairs gives the most favorable configuration. In particular, the structure $L^{(N/2)}=(\uparrow\rightarrow)^{(N/2)}$ is the lowest energy structure for fields pointing in hard-axis directions $\psi=\pi/4$ in the limit of infinite H. The state with higher magnetization than $L^{(N/2)}$ for fields pointing closer to the easy axis direction, $0\leqslant\psi<\pi/4$, and with the smallest expense of exchange energy is in our notation $L^{(N/2-1)}F$. The saturated state $\mathrm{FM}\equiv F^{(N/2)}$ is the most favorable state which is reached whenever energy can be gained in external fields by flipping more moments into position $\uparrow$ in the states $L^{(N/2-1)}F$, $F^{(1)}$, or $L^{(1)}X^{(1)}$. Thus, for general N we have only the following phases for infinite positive fourfold anisotropy: AF or SF as zero-field ground states; for fields with orientation close to the hard direction, $\psi=(\pi/4)$, $L^{(1)}$ and $L^{(N/2)}$; otherwise, in intermediate fields two degenerate phases $F^{(1)}$ and $L^{(1)}X^{(1)}$; at high fields an asymmetric $L^{(N/2-1)}F$ phase and the fully saturated ferromagnetic phase FM. We did numerical checks to ascertain that no further energetically stable phases do exist in external fields of arbitrary strength and direction, indeed. Thus, we searched for the states of lowest energy by sampling all possible configurations for models with $N=4,\ldots,12$ corroborating our arguments. Based on this set of magnetic configurations the resulting (H_x,H_y) phase diagram for general $N>4$ can be calculated analytically (Fig. 13). As in the simpler case of Fig. 12 for the two-layer system all these states are separated by infinitely high potential barriers and remain metastable for arbitrary fields. The first-order transitions between different phases occur along straight lines as shown in Fig. 13.

For finite strength of the fourfold anisotropy and under the influence of the exchange interactions, the basic structures are derived from the phases in Fig. 13. Under the influence of the field, they are elastically distorted into spatially *inhomogeneous* configurations. We have numerically investigated models for such cases with $N=4,\ldots,20$ and various values of anisotropy K. Figure 14 displays the general features for the example $N=8$. The numerically calculated magnetization curves corresponding to the lowest energy states for sufficiently high anisotropies show the sequence of phases present in the infinite-anisotropy phase diagram (Fig. 13). However, the degeneracy of these phases is lifted because the distortions possible at finite anisotropy yield different gains of energy for the different configurations of the phases $L^{(1)}$, $F^{(1)}$, and $L^{(1)}X^{(1)}$. Generally, depending on field orientation, large domains with nearly spin-flop-like configurations $\mathbf{l}\perp\mathbf{H}$ are favored because these configurations can be more easily distorted by the fields yielding a corresponding gain of energy. In particular, phases derived from the ferrimagnetic collinear $F^{(1)}$ phase are disfavored compared to the $L^{(1)}X^{(1)}$-type phases. The nearly collinear ferrimagnetic configurations seem to exist only as metastable states. For fields closer to the hard-axis direction the phases with either one L pair or $N/2$ L pairs occur. Under the influence of an applied field further discontinuous transitions occur at intermediate anisotropies, as seen, e.g., in Fig. 14(a) for $K/J=0.375$. These transitions are jumps from one energy basin to another, which are formed by distorting degenerate configurations mainly of the type $L^{(1)}$ and $L^{(1)}X^{(1)}$.

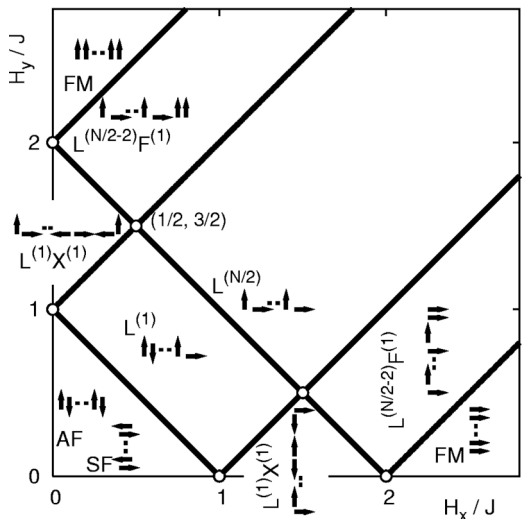

FIG. 13. (H_x,H_y) phase diagram of the multilayer in the limit of infinite positive fourfold anisotropy. The phase region of the $L^{(1)}X^{(1)}$ phases coincides with that of the collinear ferrimagnetic $F^{(1)}$, not shown here. (For details see text.)

At low anisotropies the phase diagram attains the behavior discussed for zero anisotropies in Sec. III. Here the magnetic states are only influenced by the cuts of exchange bonds at the surfaces and spatially inhomogeneous spin-flop states slightly distorted by fourfold anisotropy are realized (see Figs. 2 to 4). (H_x,H_y) diagrams for this isotropic case consist of the region of the inhomogeneous SF phase (Figs. 2 and 3) separated from the saturated flip state by the critical line $H_e^{(N)}$ (Fig. 6). These global features of the phase diagrams are similar to the case of antiferromagnetic multilayers with uniaxial anisotropy.[8]

Up to now we have discussed the effects of the competition between the bilinear exchange and fourfold anisotropy. It is clear that finite *biquadratic coupling* may substantially

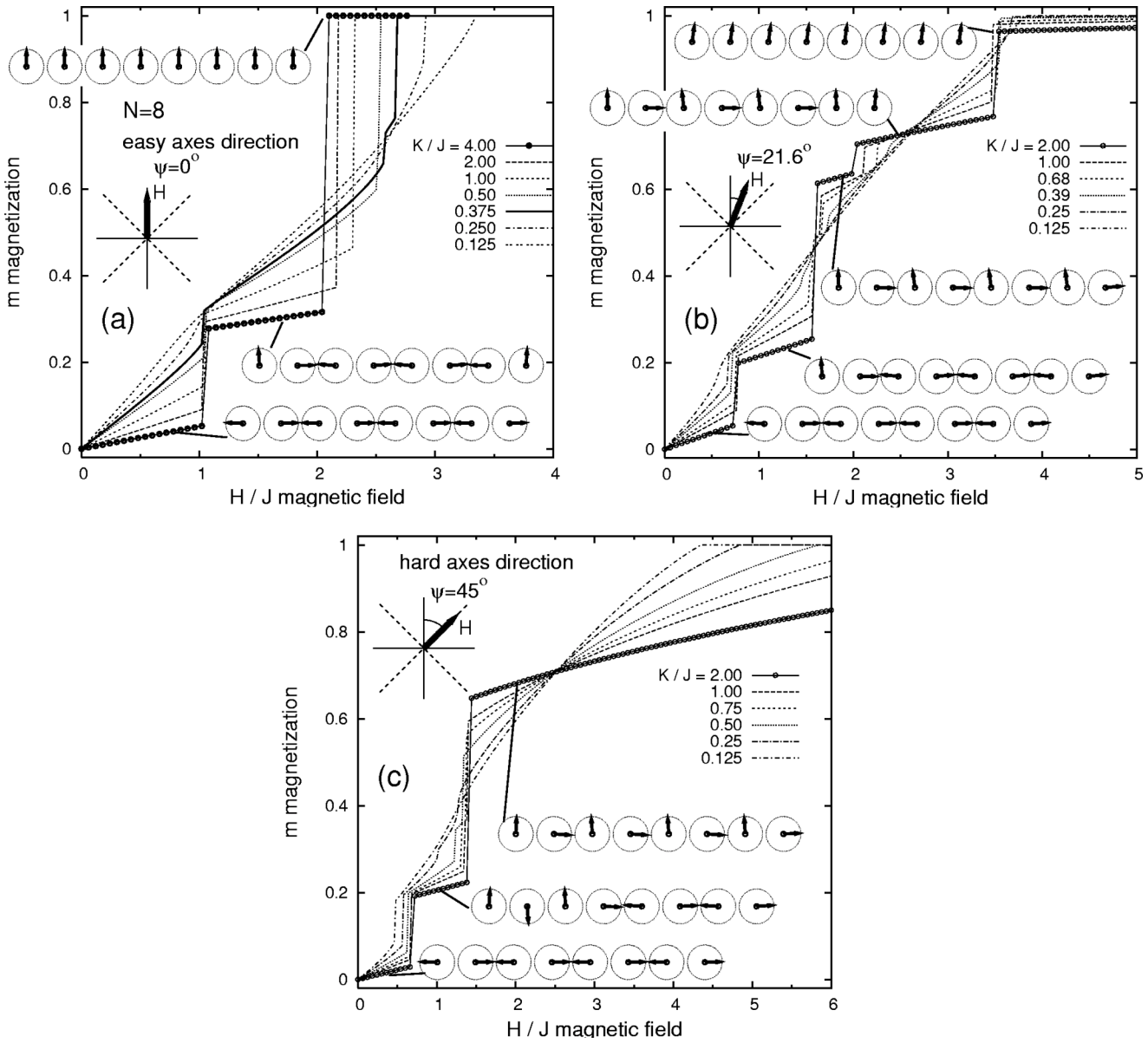

FIG. 14. Examples of magnetization in an antiferromagnetic multilayer with $N=8$. Curves corresponding to the evolution of lowest energy states and for various values of anisotropy are shown with field oriented in directions of an easy axis (a), in an oblique field (b), and in hard-axis direction (c). ψ is angle between magnetic field and easy-axis direction. In each case, various magnetic configurations are shown for the discontinuous evolution of the magnetization curves with highest anisotropy.

change the critical fields and stability regions of the various phases as it affects the elastic stiffness of the system. We note further that the simple structure of the phase diagram ruled by the phases present in the infinite-anisotropy limit of Fig. 13 is valid only for the case of equal exchange constants $J_i \equiv J$ in the multilayer stack. For arbitrary sets of values for J_i in energy (1) the phase diagrams may become considerably more complex and may contain further phases with different combinations of flipped 90° and 180° spin pairs. Even in such cases, the outline of the magnetic phase diagrams, described here for finite equal-constant superlattices, should generally hold. (i) The high-anisotropy limit is comparably simple with few phases determined by the competing lowest-energy basins of the anisotropy. Nonequal constants may lift some degeneracies that are present in superlattices. (ii) In intermediate anisotropy range many elastically distorted phases appear, which are derived from stable and metastable high-anisotropy phases. (iii) For vanishing anisotropy the phase diagrams become simple again as only inhomogeneous spin-flop-like phases and the saturated ferromagnetic phase remain in external fields.

B. Magnetization processes in real systems

So far, we have analyzed single-domain magnetic configurations. Magnetization processes in real systems, however, are usually accompanied by complex reconstruction of the multidomain patterns as those recently observed in Fe/Cr multilayers.[20,21]

There are two main physical mechanisms for multidomain states in the systems under discussion. Fourfold degeneracy of the ground state leads to creation of *antiferromagnetic multidomain structures* with 90° domain walls. Unlike the case of magnetic materials with nonzero total magnetization, where multidomain states are caused by demagnetization effects, in antiferromagnets such domains are *metastable* and arise during the formation of the ordering state, i.e., they have a kinetic origin.[44] Hence, multidomain patterns observed in antiferromagnetic coupled two-layers and multilayers have irregular morphologies and depend on thermal and magnetic-field histories.[25]

However, another type of multidomain structures arises in the vicinity of field-induced discontinuous transitions.[31] Such thermodynamically stable *transitional domain structures* are formed by domains from states corresponding to the coexisting phases at first-order transitions. These domains are analogous to the domains of a demagnetized ferromagnet. In principle, the equilibrium parameters of such multidomain structures and their boundaries can be calculated by standard methods.[31,25] In Ref. 30 such calculations have been carried out for bulk easy-plane tetragonal antiferromagnets. *Magnetoelastic interactions* lead to modification of the inhomogeneous states and decrease the regions of the multidomain states up to their complete suppression.[25,31,45] This and other coercivity mechanism partly block the development of the equilibrium states. As a result, in real systems the evolution of multidomain states[20,21] is accompanied by rather strong hystereses.[9] For experiments, there are two important consequences related to the starting states and history dependence of magnetization processes. The ''texture'' of a real antiferromagnetic state in zero field depends on the detailed kinetics imposed by, e.g., cooling rates or deposition conditions. On the other hand, field cycling by inner loops for an antiferromagnetic multilayer may yield various metastable configurations and multidomain structures owing to the very wide coexistence region of the domains whenever sizable magnetic anisotropies are present in the multilayer stack.

VI. CONCLUSIONS

Within a phenomenological approach we develop the theory of reorientation transitions in antiferromagnetically coupled superlattices with in-plane magnetization. Detailed investigations of the surface effects in the isotropic multilayers (Sec. III) and four-fold anisotropy effects in two-layer systems (Sec. IV) reveal the most important features of the system: (i) Complex evolution of the inhomogeneous states (Figs. 2–4) is imposed by the strong disbalance of the exchange coupling, i.e., by the *cut of the exchange bonds*. (ii) Remarkable field-induced reorientational processes occur due to enhanced four-fold anisotropy (Figs. 8–14).

The model used here, corresponding solutions and phase diagrams include as special cases earlier theoretical studies on surface[24] and fourfold anisotropy[23,30] effects. The results are in essential accordance with existing experimental observations on inhomogeneous distribution in the spin-flop phase near the saturation field,[18] and some effects of fourfold anisotropy in Co/Cu(001) wedged two-layers[9] and Fe/Cr superlattices.[16] Our approach and results enable a *qualitative* analysis of the magnetization processes in the multilayered systems (Sec. V). In spite of the rather complex phase diagrams of these systems, the analysis can be extended towards a quantitative description of real systems belonging to the class of artificial layered antiferromagnets described by Eq. (1).

So far most experimental work is carried out only for special conditions, often data are collected only with fields along easy axes. These results only cover small regions of the (H_x, H_y) phase diagrams (Figs. 10–13) and do not capture the rich varieties of magnetization processes in such systems. It is remarkable that many interesting effects, such as 90° folded phases, transitions into asymmetric canted phases, etc., are present already in antiferromagnetically coupled two-layers.[9] As we have seen, phase diagrams for multilayer systems with $N>2$ become very complex. Hence, systems with few layers are probably a better starting point for detailed investigations on magnetization processes. Such experiments could be used to assess magnetic parameters and quality of such systems. Generally, magnetization processes and checks for their dependence on magnetic and thermal prehistory should be made by applying fields in oblique directions and/or under rotating fields. Only then, the behavior of the (H_x, H_y) phase diagrams can be usefully compared with detailed theoretical investigations.

Further theoretical work may address models with nonequal constants. Also effectively ferrimagnetic systems with odd numbers N of layers and with different layer thicknesses may be interesting. Some experimental data for magnetization processes in such systems exist, e.g., for Co/Cr two-layers with different ferromagnetic layers thicknesses,[14] and for odd-numbered multilayers.[9] Interesting reorientational effects should arise also in magnetic fields, which are applied perpendicular or under arbitrary angle to the layer plane. Antiferromagnetically coupled superlattices may also undergo transitions into perpendicularly magnetized states for certain thicknesses of the individual ferromagnetic layers, as observed for Co/Cr(001).[12] In such cases the stray field must be taken into account already for laterally homogeneous states.

Concluding, we state that the magnetic effects and phenomena discussed in this paper can be used for detailed investigations on such aspects of nanomagnetism as interlayer-exchange interactions, reorientational, and multidomain processes.

ACKNOWLEDGMENTS

A.N.B. thanks H. Eschrig for support and hospitality at IFW Dresden. We thank Sächsisches Staatsministerium für Wissenschaft und Kunst for financial support.

*Corresponding author. Electronic address: u.roessler@ifw-dresden.de

†Permanent address: Donetsk Institute for Physics and Technology, 340114 Donetsk, Ukraine. Electronic address: bogdanov@kinetic.ac.donetsk.ua

[1] G.J. Strijkers, S.M. Zhou, F.Y. Yang, and C.L. Chien, Phys. Rev. B **62**, 13 896 (2000); K.Y. Kim, S.H. Jang, K.H. Shin, H.J. Kim, and T. Kang, J. Appl. Phys. **89**, 7612 (2001); A. Moser, K. Takano, D.T. Margulies, M. Albrecht, Y. Sonobe, Y. Ikeda, S.H. Sun, and E.E. Fullerton, J. Phys. D **35**, R157 (2002).

[2] M.A. Howson, B.J. Hickey, J. Xu, D. Greig, P. Rhodes, and N. Wiser, Phys. Rev. B **49**, 9560 (1994).

[3] R.W. Wang, D.L. Mills, E.E. Fullerton, J.E. Mattson, and S.D. Bader, Phys. Rev. Lett. **72**, 920 (1994); S.G.E. te Velthuis, J.S. Jiang, S.D. Bader, and G.P. Felcher, *ibid.* **89**, 127203 (2002).

[4] P. Steadman, M. Ali, A.T. Hindmarch, C.H. Marrows, B.J. Hickey, S. Langridge, R.M. Dalgliesh, and S. Foster, Phys. Rev. Lett. **89**, 077201 (2002); S.G.E. te Velthuis, J.S. Jiang, and G.P. Felcher, Appl. Phys. Lett. **77**, 2222 (2000).

[5] O. Hellwig, T.L. Kirk, J.B. Kortright, A. Berger, and E.E. Fullerton, Nat. Mater. **2**, 112 (2003).

[6] K. Ounadjela, D. Muller, A. Dinia, A. Arbaoui, P. Panissod, and G. Suran, Phys. Rev. B **45**, 7768 (1992); S. Hamada, K. Himi, T. Okuno, and K. Takanashi, J. Magn. Magn. Mater. **240**, 539 (2002).

[7] H. Itoh, H. Yanagihara, K. Suzuki, and E. Kita, J. Magn. Magn. Mater. **257**, 184 (2003).

[8] A.N. Bogdanov and U.K. Rößler, Phys. Rev. B **68**, 012407 (2003); U.K. Rößler and A.N. Bogdanov, *ibid.* **69**, 094405 (2004).

[9] K. Bröhl, S. Di Nunzio, F. Schreiber, Th. Zeidler, and H. Zabel, J. Appl. Phys. **75**, 6184 (1994); K. Bröhl, Th. Zeidler, F. Schreiber, A. Schreyer, and H. Zabel, J. Magn. Magn. Mater. **130**, L1 (1994).

[10] A. van der Graaf, M. Valkier, J. Kohlhepp, and F.J.A. den Broeder, J. Magn. Magn. Mater. **165**, 157 (1997).

[11] R.W.E. van de Kruijs, M.Th. Rekveldt, H. Ferdrikze, J.T. Kohlhepp, J.K. Ha, and W.J.M. de Jonge, Phys. Rev. B **65**, 064440 (2002).

[12] T. Zeidler, F. Schreiber, and H. Zabel, J. Appl. Phys. **79**, 4793 (1996).

[13] J.J. Picconatto, M.J. Pechan, and E.E. Fullerton, J. Appl. Phys. **81**, 5058 (1997).

[14] J.Z. Hilt, J.J. Picconatto, A. O'Brien, M.J. Pechan, and E.E. Fullerton, J. Magn. Magn. Mater. **198-1999**, 387 (1999).

[15] M. Rührig, R. Schäfer, A. Hubert, R. Mosler, J.A. Wolf, S. Demokritov, and P. Grünberg, Phys. Status Solidi A **125**, 635 (1991).

[16] V.V. Ustinov, M.A. Milyaev, L.N. Romashev, T.P. Krinitsina, and E.A. Kravtsov, J. Magn. Magn. Mater. **226-230**, 1811 (2001).

[17] C. Chesman, M.A. Lucena, M.C. de Moura, A. Azevedo, F.M. de Aguiar, S.M. Rezende, and S.S.P. Parkin, Phys. Rev. B **58**, 101 (1998).

[18] V. Lauter-Pasyuk, H.J. Lauter, B.P. Toperverg, L. Romashev, and V. Ustinov, Phys. Rev. Lett. **89**, 167203 (2002); V. Lauter-Pasyuk, H.J. Lauter, B. Toperverg, L. Romashev, M. Minayev, A. Petrenko, V. Aksenov, and V. Ustinov, J. Magn. Magn. Mater. **258-259**, 382 (2003).

[19] K. Temst, E. Kunnen, V.V. Moshchalkov, H. Maletta, H. Fritzsche, and Y. Bruynseraede, Physica B **276-278**, 684 (2000).

[20] D.L. Nagy, L. Bottýan, B. Croonenborghs, L. Deák, B. Degroote, J. Dekoster, H.J. Lauter, V. Lauter-Pasyuk, O. Leupold, M. Major, J. Meersschaut, O. Nikonov, A. Petrenko, R. Rüffer, H. Spiering, and E. Szilágyi, Phys. Rev. Lett. **88**, 157202 (2002); L. Bottýan, L. Deák, J. Dekoster, E. Kunnen, G. Langouche, J. Meersschaut, M. Major, D.L. Nagy, H.D. Rüter, E. Szilágyi, and K. Temst, J. Magn. Magn. Mater. **240**, 514 (2002).

[21] H. Lauter, V. Lauter-Pasyuk, B. Toperverg, L. Romashev, M. Milyaev, T. Krinitsina, E. Kravtsov, V. Ustinov, A. Petrenko, and A. Aksenov, J. Magn. Magn. Mater. **258-259**, 338 (2003).

[22] S.O. Demokritov, J. Phys. D **31**, 925 (1998).

[23] B. Dieny, J.P. Gavigan, and J.P. Rebouillat, J. Phys.: Condens. Matter **2**, 159 (1990); B. Dieny and J.P. Gavigan, *ibid.* **2**, 187 (1990).

[24] F.C. Nörtemann, R.L. Stamps, A.S. Carriço, and R.E. Camley, Phys. Rev. B **46**, 10 847 (1992); A.L. Dantas and A.S. Carriço, *ibid.* **59**, 1223 (1999).

[25] A. Hubert and R. Schäfer, *Magnetic Domains* (Springer-Verlag, Berlin, 1998).

[26] D.L. Mills, J. Magn. Magn. Mater. **198-199**, 334 (1999).

[27] P. Grünberg, R. Schreiber, Y. Pang, M.B. Brodsky, and H. Sowers, Phys. Rev. Lett. **57**, 2442 (1986); S.S.P. Parkin, N. More, and K.P. Roche, *ibid.* **64**, 2304 (1990).

[28] M.D. Stiles, J. Magn. Magn. Mater. **200**, 322 (1999).

[29] Yu.V. Goryunov, N.N. Garif'yanov, G.G. Khaliullin, I.A. Garifullin, L.R. Tagirov, F. Schreiber, Th. Mühge, and H. Zabel, Phys. Rev. B **52**, 13 450 (1995).

[30] A.N. Bogdanov, Fiz. Tverd. Tela **32**, 1749 (1990) [Sov. Phys. Solid State **32**, 1018 (1990)]; A.N. Bogdanov and I.E. Dragunov, Low Temp. Phys. **24**, 852 (1998).

[31] V.G. Bar'yakhtar, A.N. Bogdanov, and D.A. Yablonskii, Usp. Fiz. Nauk. **156**, 47 (1988) [Sov. Phys. Usp. **31**, 810 (1988)].

[32] L.D. Landau and E.M. Lifshitz, *Statistical Physics*, Course of Theoretical Physics Vol. 5 (Butterworth-Heinemann, Oxford, 1980).

[33] S.-K. Kim and J.B. Kortright, Phys. Rev. Lett. **86**, 1347 (2001); F. Wilhelm, P. Poulopoulos, G. Ceballos, H. Wende, K. Baberschke, P. Srivastava, D. Benea, H. Ebert, M. Angelakeris, N.K. Flevaris, D. Niarchos, A. Rogalev, and N.B. Brookes, *ibid.* **85**, 413 (2000).

[34] A.N. Bogdanov and U.K. Rößler, Phys. Rev. Lett. **87**, 037203 (2001); A.N. Bogdanov, U.K. Rößler, and K.-H. Müller, J. Magn. Magn. Mater. **238**, 155 (2002).

[35] A. Thiaville and A. Fert, J. Magn. Magn. Mater. **113**, 161 (1992).

[36] M.T. Johnson, P.J.H. Bloemen, F.J.A. den Broeder, and J.J. de Vries, Rep. Prog. Phys. **59**, 1409 (1996).

[37] W.H. Press, S.A. Teukolsky, W.T. Vetterling, and B.P. Flannery, *Numerical Recipes in C*, 2nd ed. (Cambridge University Press, Cambridge, 1992), Chap. 10.6.

[38] A.I. Mitsek, N.P. Kolmakova, and D.I. Sirota, Fiz. Met. Metalloved. **38**, 35 (1974).

[39] A.N. Bogdanov and I.Ya. Granovskii, Fiz. Tverd. Tela **29**, 2913 (1987) [Sov. Phys. Solid State **29**, 1674 (1987)].

[40] F.Y. Wu, Rev. Mod. Phys. **54**, 235 (1982).

[41] K.-H. Müller and V.N. Narozhnyi, Rep. Prog. Phys. **64**, 943 (2001); P.C. Canfield and S.L. Bud'ko, J. Alloys Compd. **262**, 169 (1997); G. André, F. Bourée, M. Kolenda, B. Leśniewska, A. Olés, and A. Szytuła, Physica B **292**, 176 (2000).

[42] P.C. Canfield, S.L. Bud'ko, B.K. Cho, A. Lacerda, D. Farrell, E. Johnston-Halperin, V.A. Kalatsky, and V.L. Pokrovsky, Phys. Rev. B **55**, 970 (1997); V.A. Kalatsky and V.L. Pokrovsky, *ibid.* **57**, 5485 (1998).

[43] K.D. Myers, P.C. Canfield, V.A. Kalatsky, and V.L. Pokrovsky, Phys. Rev. B **59**, 1121 (1999).

[44] A. Hubert, *Theorie der Domänenwände in Geordneten Medien* (Springer, Berlin, 1974).

[45] A.N. Bogdanov, A. DeSimone, S. Müller, and U.K. Rößler, J. Magn. Magn. Mater. **261**, 204 (2003).